APPLICATION OF DEEP LEARNING APPROACH IN TRANSCRANIAL MAGNETIC STIMULATION FOR PREDICTING ELECTRIC FIELD

By

Khaleda Akhter Sathi, MSc Eng

19METE013P

A thesis submitted in partial fulfilment of the requirements for the degree of MASTER of SCIENCE in ELECTRONICS AND TELECOMMUNICATION ENGINEERING

Department of Electronics and Telecommunication Engineering

CHITTAGONG UNIVERSITY OF ENGINEERING AND TECHNOLOGY

APRIL 2023

Declaration

I hereby declare that the work contained in this Thesis has not been previously submitted to meet requirements for an award at this or any other higher education institution. To the best of my knowledge and belief, the Thesis contains no material previously published or written by another person except where due reference is cited. Furthermore, the Thesis complies with PLAGIARISM and ACADEMIC INTEGRITY regulation of CUET.

Khaleda Akhter Sathi
19METE013P
Department of Electronics and Telecommunication Engineering
Chittagong University of Engineering & Technology (CUET)

Dedication

To my beloved parents,

Md. Khorshed Alam and Kohinoor Alam

for their sacrifices, endearment, and eternal support at every difficulty.

List of Publications

Journal Article

- Publication 1: Khaleda Akhter Sathi, Md Kamal Hosain, Md. Azad Hossain, and Abbas Z Kouzani, "Attention-Assisted Hybrid 1D CNN-BiLSTM Model for Predicting Electric Field Induced by Transcranial Magnetic Stimulation Coil", *Scientific reports 13, 2494, 2023.* 10.1038/s41598-023-29695-6.
- Publication 2: Khaleda Akhter Sathi, Md Kamal Hosain, and Md. Azad Hossain, "Analysis of Induced Field in the Brain Tissue by Transcranial Magnetic Stimulation Using Halo-V Assembly Coil", *Neurology Research International,* 1-10. 2022. 10.1155/2022/7424564.
- Publication 3: K. A. Sathi, M. A. Hossain, M. K. Hosain, N. H. Hai and M. A. Hossain, "A Deep Neural Network Model for Predicting Electric Fields Induced by Transcranial Magnetic Stimulation Coil," *IEEE Access*, vol. 9, pp. 128381-128392, 2021, 10.1109/ACCESS.2021.3112612.

Approval/Declaration by the Supervisor

This is to certify that KHALEDA AKHTER SATHI has carried out this research work under my supervision, and that he has fulfilled the relevant Academic Ordinance of the Chittagong University of Engineering & Technology, so that he is qualified to submit the following Thesis in the application for the degree of MASTER of SCIENCE in ELECTRONICS AND TELECOMMUNICATION ENGINEERING. Furthermore, the Thesis complies with the PLAGIARISM and ACADEMIC INTEGRITY regulation of CUET.

Dr. Md. Azad Hossain

Professor

Department of Electronics and Telecommunication Engineering

Chittagong University of Engineering & Technology

Acknowledgment

BISMILLAHIR RAHMANIR RAHIM,

I am grateful to Almighty Allah for giving the good health and well-being that were necessary to work on this research. I wish to express my sincere thanks to Dr. Md. Azad Hossain, supervisor of my thesis, Professor of the Department, Electronics and Telecommunication Engineering, and co-supervisor Dr. Md. Kamal Hosain, Professor, Department of Electronics & Telecommunication Engineering, Rajshahi University of Engineering & Technology, for providing me with all the necessary facilities for the research. I am extremely thankful and indebted to them for sharing expertise, and sincere and valuable guidance and encouragement extended to me. I also want to thank all the faculty members of the department for their help and support. I am also thankful to my classmates and lab technicians.

In addition, I take this opportunity to express gratitude to my parents, family members, my fellow classmates for the unceasing encouragement, support and attention throughout my whole life which helped me to write this thesis.

Abstract

As a non-invasive neuromodulation technique, transcranial magnetic stimulation (TMS) has already exhibited a great impact in clinical applications and scientific researches. For finding new clinical applications of TMS, the current study focused on a deep learning-based prediction model as an alterative of time-consuming electromagnetic (EM) simulation software. However, the main bottleneck of the existing prediction models is to consider fewer input parameters such as single coil type and coil position for predicting electric field value. To address these limitations, this research develops an improved approach based on a deep neural network (DNN) to predict electric field by considering several input parameters such as coil turns of single wing, coil thickness, coil diameter, distance between two wings, distance between head and coil position, and angle between two wings of coil. In addition, considering the fact of focality and depth tradeoff, the assembly coil is designed. The performance of the model is evaluated based on four verification statistic metrics including coefficient of determination (R^2), mean squared error (MSE), mean absolute error (MAE), and root mean squared error (RMSE) between the simulated and predicted values. Compared to current state-of-the-art methods, the proposed DNN model outperformed with the value of R2=0.9992, MSE=0.0005, MAE=0.0188, and RMSE=0.0228 in the testing stage. Therefore, the proposed DNN model can accurately predict electric field from assembly coil in a lower period of time without using traditional simulation software.

বিমূর্ত

একটি অ-আক্রমণাত্মক নিউরোমোডুলেশন কৌশল হিসাবে, ট্রান্সক্রানিয়াল ম্যাগনেটিক স্টিমুলেশন (টিএমএস) ইতিমধ্যেই ক্লিনিকাল ব্যবহার এবং বৈজ্ঞানিক গবেষণায় একটি দুর্দান্ত প্রভাব প্রদর্শন করেছে। টিএমএস এর নতুন ক্লিনিকাল ব্যবহার সন্ধানের জন্য, বর্তমান গবেষণা সময় সাপেক্ষ ইলেক্ট্রোম্যাগনেটিক (ইএম) সিমুলেশন সফ্টওয়্যারের বিকল্প হিসাবে একটি ডিপ লার্নিং-ভিত্তিক ভবিষ্যদ্বাণী মডেলের উপর দৃষ্টি নিবদ্ধ করে। তবে, বিদ্যমান ভবিষ্যদ্বাণী মডেলের প্রধান সমস্যা হল বৈদ্যুতিক ক্ষেত্রের মান পূর্বাভাস করার জন্য ইনপুট প্যারামিটার যেমন একক কয়েল টাইপ এবং কয়েলের অবস্থান বিবেচনা করা। এই সীমাবদ্ধতাগুলিকে মোকাবেলা করার জন্য, এই গবেষণাটি একটি ডিপ নিউরাল নেটওয়ার্ক (ডিএনএন) এর উপর ভিত্তি করে একটি উন্নত পদ্ধতির বিকাশ করে যাতে একাধিক ইনপুট প্যারামিটার যেমন একক কয়েল বাঁক, কয়েলের পুরুত্ব, কয়েলের ব্যাস, মাথা থেকে দুটি কয়েলের মধ্যে দূরত্ব, এবং কয়েলের অবস্থান, এবং কয়েল দুটি মধ্যে কোণ বিবেচনা করে বৈদ্যুতিক ক্ষেত্রের পূর্বাভাস করে। উপরন্তু, ফোকালিটি এবং গভীরতার ভারসাম্য বিষয়টি বিবেচনা করে, অ্যাসেম্বলি কয়েল ডিজাইন করা হয়েছে। মডেলটির কার্যকারিতা মূল্যায়ন করা হয় চারটি যাচাইকরণ পরিসংখ্যান মেট্রিক্সের উপর ভিত্তি করে যার মধ্যে রয়েছে নির্ণয়ের সহগ (আর2), গড় বর্গ ত্রুটি (এমএসই), গড় পরম ত্রুটি (এমএই), এবং সিমুলেটেড এবং পূর্বাভাসিত মানগুলির মধ্যে রুট গড় স্কোয়ার ত্রুটি (আরএমএসই)। বর্তমান অত্যাধুনিক পদ্ধতির তুলনায়, প্রস্তাবিত ডিএনএন মডেলটি পরীক্ষার পর্যায়ে আর2=০.৯৯৯২, এমএসই=০.০০০৫, এমএই=০.০১৮৮, এবং আরএমএসই=০.০২২৮ মানের সাথে উন্নয়ন করেছে। অতএব, প্রস্তাবিত ডিএনএন মডেলটি প্রথাগত সিমুলেশন সফ্টওয়্যার ব্যবহার না করে কম সময়ের মধ্যে অ্যাসেম্বলি কয়েল থেকে বৈদ্যুতিক ক্ষেত্রের সঠিকভাবে পূর্বাভাস দিতে পারে।

Table of Contents

List of Figures

List of Tables

Table No. **Table Caption** **Page No.**

Chapter 1: INTRODUCTION

This chapter outlines the background (section 1.1) of the research and its problem statement (section 1.2). Next, section 1.3 describes the purpose of this research. Finally, section 1.4 includes an outline of the remaining chapters of the Thesis.

1.1 RESEARCH BACKGROUND

Transcranial magnetic stimulation (TMS) has shown an effective therapeutic outcome for some neural disorders such as major depressive disorder, traumatic brain injury, parkinson's disease, post-traumatic stress disorder, etc. [1-4]. The TMS technique requires a magnetic coil normally placed on the subject's head that is fed with a high-valued short-duration current pulse [5]. The electric current conveyed in the coil produces a magnetic field that results in an induced electric field inside the brain tissues [6]. Then a localized axial depolarization is formed by the induced electrical field in the underlying cortical tissue which has a therapeutic effectiveness of neural disorders [7]. To ensure a greater therapeutic effect, the induced electric field should have to be strong enough so that it can depolarize the target neurons that are responsible for the neural disorders [8, 9]. Moreover, some other factors including focality (area of stimulation) and depth (distance from vertex) of the induced electric field are associated with the effectiveness of TMS treatment. The commercially available single coils named as Fig.-eight, halo, circular, double cone, H, etc. are suffering from the trade-off between stimulation focality and depth. For instance, the Fig.-eight coil aims to generate a concentrated electric field within a smaller region rather than stimulating the deeper brain structure. Alternatively, the H-coil increases the stimulation depth by maintaining a moderate focality. The Halo coil also stimulates the deep brain structure but it degrades the focality. Thus, in the

recent research the development of an assembly coil (combination of single coils) is emphasized to maintain a trade-off between stimulation depth and focality [10].

1.2 PROBLEM STATEMENT

The TMS induced electric field intensity is highly sensitive to numerous factors such as subject head anatomy, coil positioning, coil configuration, etc. An iterative computer simulation is required to determine the desired electric field intensity inside the brain tissues. However, the problem associated with the electric field enumeration is the computational time that is generally high for the commercial electromagnetic (EM) simulation software such as SimNIBS, Sim4Life, and COMSOL Multiphysics [11, 12]. Moreover, the computational time is related to the development of a human head model and the determination of the electric field with the aid of a volume conductor model [13, 14]. The important bottleneck is that it takes few hours to half a day to design a TMS coil on a human head model as well as to compute the electric field.

1.3 AIMS AND OBJECTIVES

- To design an optimum coil for providing an effective treatment of the neurological disorder patients by assuring a tradeoff between depth and focality in the induced electric field.
- To develop a database considering several coil designing parameters such as coil turns of single wing, coil thickness, coil diameter, distance between two wings, distance between head and coil position, and angle between two wings of coil.
- To apply the deep learning algorithms for optimum electric field prediction in assembly transcranial magnetic stimulation coil by analyzing different coil parameters.

- To investigate the computational cost of estimating electric field for different coils.

1.4 THESIS CONTRIBUTIONS

- An assembly coil named HVA as a neurostimulating coil is designed that can limit the induced field within a lesser region of the scalp as well as the cortical region to enhance the stimulation focality.
- A DNN approach as a nonlinear regression model is proposed to predict the induced electric field value from assembly TMS coil under high-valued and low-frequency current pulse conditions.
- An improved DNN model based on attention assisted hybrid CNN and BiLSTM is developed for further improving the prediction of induced electric feld in HVA TMS coil.

1.5 THESIS OUTLINE

Chapter 2 reviews background literature relating to TMS therapeutic techniques and and limitation of conventional TMS simulation through the electro-magnetic software.

Chapter 3 describes the development of new assembly coil and analysing its effectiveness over single and assembly coil as well.

Chapter 4 represents how to develop a simple deep learning (DL) model and the way of generating dataset for training the model to enumerate TMS induced electric field.

Chapter 5 provides the explanation of improved DL model for superior result of predicting electric field and performance evaluation over existing state-of-the-art methods.

Chapter 6 represents the summary of overall research, limilations as well as future directions.

Chapter 2: LITERATURE REVIEW

This chapter begins with reviews literature related to deep learning model based TMS electric field prediction followed by common limitations existing on the state-of-the-art models. In addition, highlights the implications from the literature and develops the conceptual framework for the study.

The application of the deep learning (DL) approach could effectively resolve the computational cost issue [15]. Generally, the DL approach uses a layered structure of algorithm called artificial neural network (ANN) to solve several problems such as classification [16-19], regression [20-22], clustering [23, 24], and prediction [25-27]. Another advanced technique over shallow ANN called deep neural network (DNN) can develop a complex non-linear relationship with higher generalization capability by employing multiple hidden layers between the input and output [28] to compute optimum induced electric field. Recently, very few researches have been reported to compute induced electric field of TMS coil in head model through DNN model. For example, Yokota et al. [11] proposed a DNN model to estimate the electric field of TMS coil in head MR images at different coil positions. They created datasets with the help of SimNIBS and FreeSurfer segmentation softwares to train and test the U-Net DNN model. The FreeSurfer software converted the MR image into a 3D head model and the SimNIBS software calculated the electric fields by the finite element method at varying positions of the Fig.-eight coil. Thereafter, the DNN model was trained with created datasets for mapping the electric field to the MR images.

In another work, Afuwape et al. [12] utilized a deep learning method to predict electric field into T1-weighted MR images with varying coil configuration. The

3D head model was generated from the MR image and the finite element analysis was performed in Sim4Life software for sixteen different coil configurations. Then the deep convolutional neural network was trained using the generated dataset to predict the electric field of TMS coils in 3D head model. Both of the models could estimate the electric field accurately within a short time. However, the segmentation process (3D head model generation) is time-consuming as well as complicated due to the generation of both brain and skull parts. It is also quite challenging to develop an accurate head structure from low contrast MR images. Besides segmentation time, both models take a longer training time to process the data with the deep network architecture. Moreover, the estimation of the electric field is done based on the single coil and single design parameter of coil positioning. Since, the induced electric field value is dependent on different coil designing parameters such as the coil turns, coil thickness, coil angle, coil diameter, etc. [29], the optimum field calculation based on these parameters is essential for a safe and effective TMS treatment. Moreover, the advantages associated with the tradeoff between focality and depth of induced electric field cannot be achieved by the single stimulation coil but can be achieved by assembly coil. Thus the electric field for assembly coils will be predicted considering several coil designing parameters.

In terms of computational time, all existing DL-based models have the capability of computing electric fields in a lower period of time. However, the data creation processes from the segmentation software presented in [11, 12] are quite challenging because it requires high contrast T1-weighted MRI brain image. It is also difficult to produce an actual human head model from low-contrast MRI images. Moreover, the time requirement for the segmentation process is also a problem. Another delimitation of these models is that the electric field estimation accuracy depends on the quality of the MRI scans that result in performance deterioration if the picture quality deteriorates [30]. The utilization of a deep network for both encoding and decoding of data can

increase time during training. Furthermore, the use of a single coil parameter such as coil position as the input parameter cannot aid a value to effectively determine the induced electric field.

Table 2.1 Summary different study of deep learning model for electrical field prediction of TMS coil.

Reference	[11]	[12]
Prediction model	U-Net	CNN
Data type	Image	Image
Total dataset	261,072	800
Coil type	single	single
Coil parameter	coil position	-
Performance evaluation matrix	Correlation coefficient, CC=0.93 Peak signal to noise ratio, PSNR=29dB Mean absolute error, MAE=6 Mean relative absolute variation, RMAD=6%	R^2 = 0.92 MAPE = 6.2%
Limitations	• Estimation of DNN model depend upon the MRI image quality. • Consider only one coil parameter such as coil position.	• Consider no coil parameter. • Estimation of DNN model depend upon the MRI image quality.

Table 2.1 summarizes the study which are based on electric field prediction of TMS coil using deep learning model. Both of the models could estimate the electric field accurately within a short time. However, the segmentation process (3D head model generation) is time-consuming as well as complicated due to the generation of both brain and skull parts. It is also quite challenging to develop an accurate head structure from low contrast MR images. Besides segmentation time, both models take a longer training time to process the data with the deep network architecture. Moreover, the estimation of the electric field is done based on the single coil and single design parameter of coil positioning. Since, the induced electric field value is dependent on different coil

designing parameters such as the coil turns, coil thickness, coil angle, coil diameter, etc. [29], the optimum field calculation based on these parameters is essential for a safe and effective TMS treatment. Moreover, the advantages associated with the tradeoff between focality and depth of induced electric field cannot be achieved by the single stimulation coil but can be achieved by assembly coil.

Thereby, in this work a simple DNN approach is proposed for the prediction of electric field induced by TMS assembly coil, which directly regresses electric field from six different coil designing parameters. This is a numerical data-driven method for predicting electric fields where the mapping of coil modeling parameters to the electric fields is achieved using a training dataset consisting of pairs of design parameters and the relative electric fields. The mapping is characterized by the model that consist of three non-linear hidden layers between the input and output layers. For the regression task, the model is trained with 100 data samples of six coil design parameters and electric field pairs. After training the deep neural network, the electric field induced by the transcranial magnetic stimulation coil is predicted directly from any TMS coil design parameter.

Chapter 3: DEVELOPMENT OF SPHERICAL HEAD MODEL AND ASSEMBLY COIL

This chapter introduces design process of a five-shell human head model followed by a geometrical structure of assembly coil named HVA as a neuro-stimulating coil. In addition, the distributions of induced magnetic and electric fields in the five-shell spherical-shaped head model are comprehensively analyzed based on the FEM. Moreover, depending on the simulation results, an evaluation of the proposed assembly coil is performed.

3.1 MATERIALS AND METHODS

3.1.1 FIVE SHELL HEAD MODEL

In this simulation, a spherical five layers model is employed to represent the human head [31]. Fig. 3.1 shows the cross-section of the modeled human head that comprised of five different anatomical layers including the scalp, skull, cerebrospinal fluid, gray matter, and white matter respectively. All layers are indicated in the inset of the three-dimensional head model of the cartesian coordinates system. The outer and inner diameters of scalp structure are 170 mm and 160 mm respectively, while the most inner tissue i.e., white matter region is modeled with the diameter of 134 mm. The thickness of four anatomical layers of scalp, skull, cerebrospinal fluid, and gray matter are 10mm, 14mm, 6mm, and 6mm respectively [31]. The inner portion of the gray matter is considered as the white matter. The working frequency of the stimulation current is generally between 2500 to 5000 Hz but the common value of 2500 Hz is adopted in this paper [32]. The electromagnetic properties of the different

tissues of the head model at an operating frequency of 2500 Hz are presented in Table 3.1.

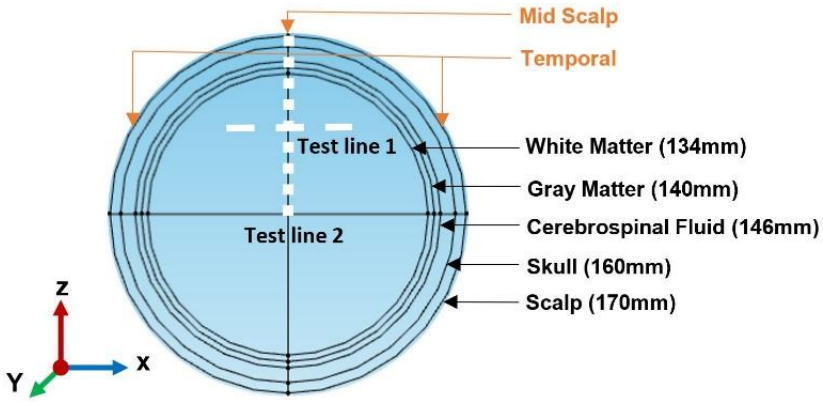

Fig. 3.1. The cross-sectional view of five layers spherical human head model.

Table 3.1 Electromagnetic properties of the five different anatomical layers at an operating frequency of 2500Hz [32].

Tissue Name	Electrical Conductivity (S/m)	Relative Permittivity	Relative Permeability
Scalp	0.0002	1140	0.99
Skull	0.0203	1440	1.00
Cerebrospinal Fluid	2	109	0.99
Gray Matter	0.104	78100	0.99
White Matter	0.0645	34300	0.99

3.1.2 COIL GEOMETRY AND EXCITATION

Fig. 3.2 shows the geometrical structure of the three coils named V, Halo, and HVA respectively. The V coil has the same dimension as the conventional fo8 coil with inner and outer diameters of 55mm and 95 mm respectively as shown in Fig. 3.2(a). The designed V coil consists of nine turns. The two wings of the V coil are separated by an angle of 45^0 which is located 5 mm above the mid-scalp of the head. The current pulse in two wings of the coil is set to flow in opposite directions. On the other hand, Fig. 3.2(b) presents the halo coil with a dimension of 175mm and 195mm for inner and outer diameter respectively. The halo coil is positioned 90 mm below the mid-scalp of the head. The direction of current flowing in the halo coil is similar to the one wings of the V coil and opposite to the other wing. The HVA coil configuration as shown in Fig. 3.2(c), consists of

two coils: a halo coil and a V coil. These two coils have a different number of turns: 9 for both wings of the V coil and 5 for the halo coil which makes a total of 23 turns. The one part of the HVA coil i.e., V coil is placed at a distance of 5 mm from the mid-scalp of the head model. The position of the V coil is set at this position to reduce unwanted tissue damage. Similarly, the other part i.e., the halo coil is placed at 90mm from the mid-scalp of the head model. The design parameters of the three coils are summarized in Table 3.2. Each of the coils is modeled by considering the torus shape of copper material with an electrical conductivity of 5.8 × 10^7 S/m. Also, the coils are fed with a current pulse of amplitude 5000 A and a frequency of 2500 Hz [32].

Table 3.2 Design parameters of three coils

Coil name	Inner diameter $\boldsymbol{d_{in}}$(mm)	Outer diameter $\boldsymbol{d_{out}}$(mm)	Total coil turns	Angle between two wings $\boldsymbol{\theta}$(degree)
V	55	95	18	45^0
Halo	175	195	5	-
HVA	V=55 Halo=175	V=95 Halo=195	23	45^0

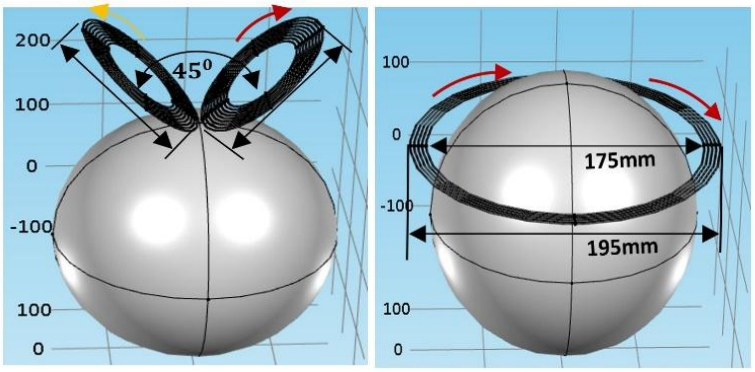

(a) (b)

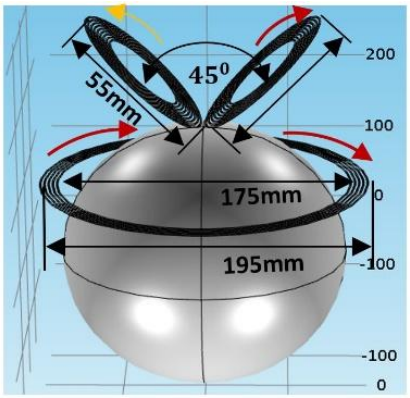

(c)

Fig. 3.2. Geometrical structure of coils. (a) V coil (b) Halo coil, and (c) HVA coil. The red arrow line indicates the clockwise current direction and the yellow arrow line indicates the anti-clockwise current direction.

3.1.3 GOVERNING EQUATION AND MESHING

The generation of fields by feeding a high amplitude current pulse to the coil follows Maxwell's fourth law of ampere's circuit law. Where the distribution of the charge carrier in the closed-loop coil generates a magnetic field that is in a direction perpendicular to the coil surface, as a result, the changing magnetic field induces an electric field in the conductive head tissue medium. The differential form of the following equations 1 to 4 is used to represent these scenarios, where J and J_e represent the current density vector and the externally generated current density respectively. The magnetic field vector and potential are indicated by H and A, whereas B is the magnetic intensity vector. Moreover, the induced electric field intensity and displacement vector are denoted as E and D respectively.

$$J = \nabla \times H = \sigma E + j\omega D + J_e \quad (1)$$

$$E = -\nabla V - j\omega A \quad (2)$$

$$\mathrm{B} = \nabla \times A \quad (3)$$

$$\mathrm{D} = \epsilon_0 \epsilon_r E \quad (4)$$

Based on the above equations the coils are simulated in COMSOL Multiphysics 5.0a software for frequency domain analysis of the electromagnetic field. The magnetic and electric field (mef) interface from AC/DC module of the COMSOL software is used for simulation. In the simulation, the total model domain including head and coil geometries are divided into several sub-domains for solving the governing equations [33]. Since the dimension of the coil is small as

compared to the head model, the mesh elements for the coil geometries are set to denser than the head tissue medium to compute the actual changes of the electric field in the conductive head tissue medium. Therefore, the fine tetrahedral meshing elements are considered with sizes ranging from 8 mm to 100 mm that ensure an effective numerical accuracy in a low computational time. Moreover, the maximum element growth rate and curvature factor are set at the value of 5 and 0.9 respectively. The complete mesh consist of domain, boundary, and edge element with numbers 139062, 40104, and 9232 respectively.

3.2 RESULTS AND ANALYSIS

The designed coils are simulated with COMSOL Multiphysics 5.0a software. In the xy plane, the surface distributions of H-field for V, halo, and HVA coils at the head tissue medium are presented in Fig. 3.3. From Fig. 3.3(a) it is shown that the magnetic field intensity of the V coil is greater at the center of the mid-scalp region because the two coil wings meet at that region. On the contrary, the mid-scalp region is free from the magnetic field induced by the halo coil as presented in Fig. 3.3(b). It produces the H-field at the temporal region of the head model. The magnetic field of the HVA coil as shown in Fig. 3.3(c) is concentrated at the lesser region of the mid-scalp as compared to the V coil. Moreover, it has a reduced H-field at the temporal region as compared to the halo coil. Therefore, the concentrated H-field with lesser area results in reducing the area of induced electric field which is responsible for the activation of unwanted head tissues.

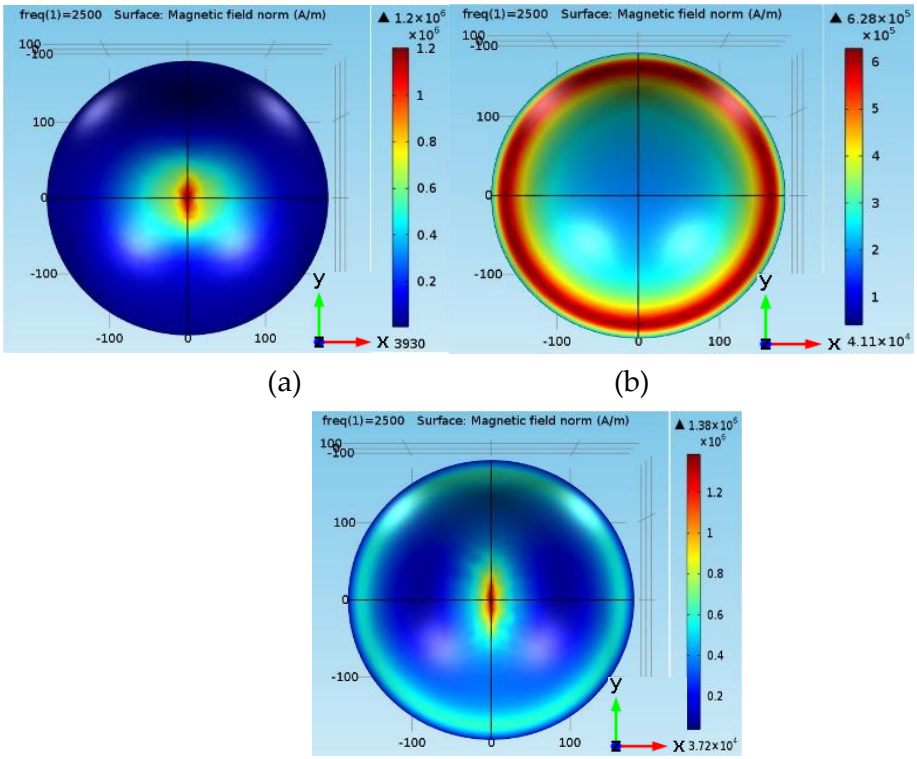

(a) (b)

(c)

Fig. 3.3. Magnetic field distribution of coils. (a) V coil, (b) Halo coil, and (c) HVA coil.

The slice views of electric field distribution for V, halo, and HVA coils in the zx plane are presented in Fig. 3.4. From Fig. 3.4(a) it is observed that the total maximum electric field value of the V coil is 312 V/m with a lower depth of stimulation in the mid-scalp region. On the other hand, the halo coil induces a total maximum electric field of 550 V/m with a greater field penetration depth at the inner region of the white matter on both left and right temporal (see Fig. 3.4(b)). This electric field is also spread over a wide region. The total maximum electric field value of the HVA coil as shown in Fig. 3.4(c) is found to be 482 V/m. It shows the similar field penetration depth of the halo coil but reducing the area of stimulation at the scalp on the temporal. Moreover, the electric field value is under the threshold in the cortex region on the mid-scalp of the head. Therefore, compared with the V coil it has greater field penetration depth and has a lower area of stimulation as compared to the halo coil.

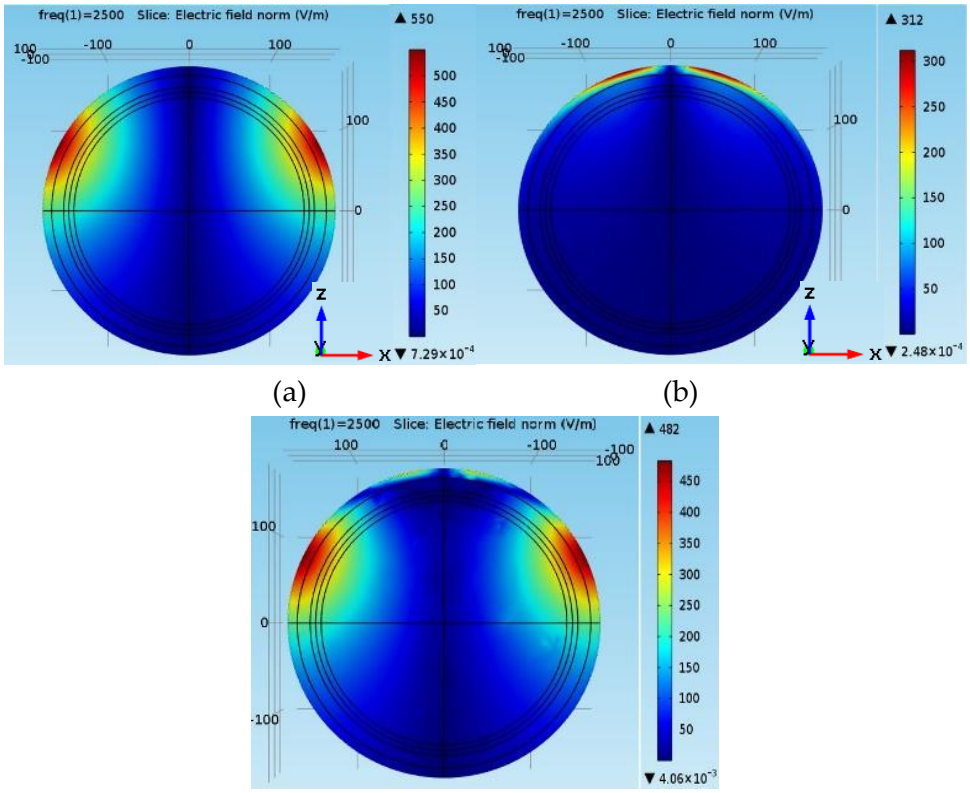

Fig. 3.4 Electric field distribution of coils. (a) V coil, (b) Halo coil, and (c) HVA coil.

The line graphs of the electric field by V, halo, and HVA coils along the test line-1 (see in Fig. 3.1) are shown in Fig. 3.5. The test line-1 is considered parallel to the x-axis with endpoints of (0, −80, 80) and (80, −80, 80) mm where the temporal region of the head model is located. The electric field induced by the V coil reaches the threshold value (>100 V/m) [23] at both endpoints of (> 70mm and < -70mm) of the test line that representing lesser field penetration depth. On the contrary, the threshold electric field intensity produced by the halo coil can stimulate the deeper region of (>25mm and <-25mm) along the test line. But the electric field curve is linearly decreased from both endpoints towards the center of the spherical head model indicating lower focality. In the case of HVA coil, the threshold electric field intensity is found at depth (>30mm and <-30mm). Thus, compared to V and halo coil, the HVA coil improves the penetration depth as well as focality within the range of -90mm to -30mm and 30 mm to 90mm respectively.

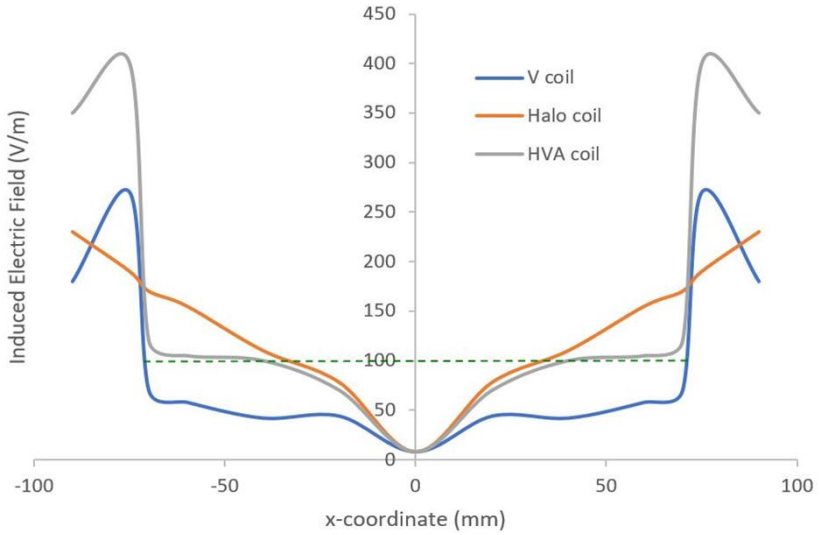

Fig. 3.5 Electric field distribution along test line 1. (green dotted line indicates the neuron stimulation threshold).

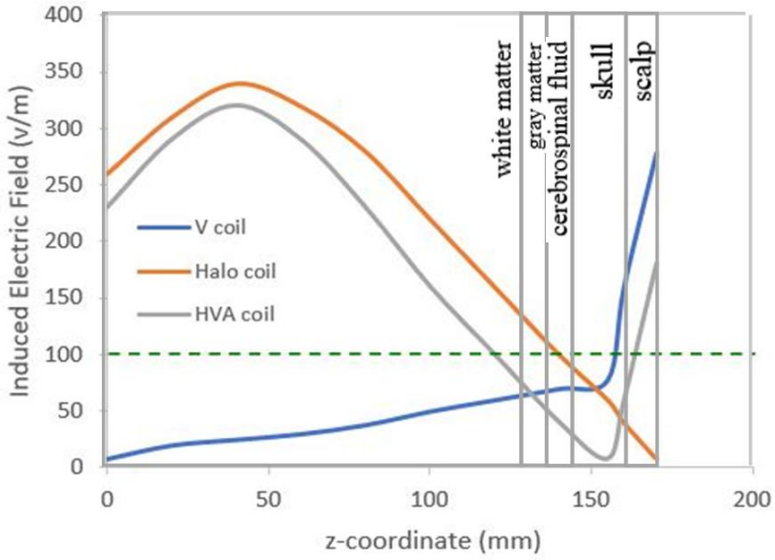

Fig. 3.6 Electric field distribution along test line 2 (green dotted line indicates the neuron stimulation threshold).

Moreover, Fig. 3.6 presents the line graph of the induced electric field for V, halo, and HVA coils along test line-2 (see Fig. 3.1). Where the test line 2 is considered along the z-axis with endpoints of (0, 0, 0) and (0, 0, 170), where the mid-scalp of the head model is located. The induced electric intensity of the V coil is higher than the threshold only at the skull surface from 155mm to 170 mm on the mid-scalp of the head and produces an under threshold electric field

intensity at the inner region of the skull below 155 mm. On the contrary, an electric field over threshold is induced by the halo coil at the region below 150mm. Hence, the skull surface of the mid-scalp is free from stimulation. For the HVA coil, the over threshold electric field intensity is induced at the skull surface from 155mm to 170 mm as well as at the deeper region below the 120mm from the top of the head. Therefore, the inner region of the white matter is stimulated by an HVA coil with a threshold electric field that indicates a suitable deeper penetration.

3.3 PERFORMANCE EVALUATION

To evaluate the performance of the designed HVA coil, its induced electric field predicted in spherical model is compared with the existing single and assembly coils in terms of the area of stimulation. The distribution of induced electric field on the surface of the scalp for four different coils i.e., V, Halo, HFA, and HVA are shown in Fig. 3.7. From the results of electric field distribution, it is clear that the stimulation area of the HVA coil is lower than the other single and assembly coil reported here. Hence HVA coil can reduce the undesired tissue excitation in the scalp region than the V, Halo, and HFA coils. Moreover, the bar plot of the maximum electric field induced by four different coils on the white matter, gray matter, and scalp region of the head model is shown in Fig. 3.8. Results show that the HVA coil stimulates the white matter region with weaker intensities than the HFA coil. However, the comparable ratios of the induced electric field in the scalp and the white matter region for both HVA and HFA coils are found as 4.99 and 2.99 respectively. In case of scalp to gray matter intensity ratio, the values are found as 4.83 and 2.54 for HVA and HFA respectively. These indicate that the HVA coil can reduce the over-stimulation of neurons near the stimulation site.

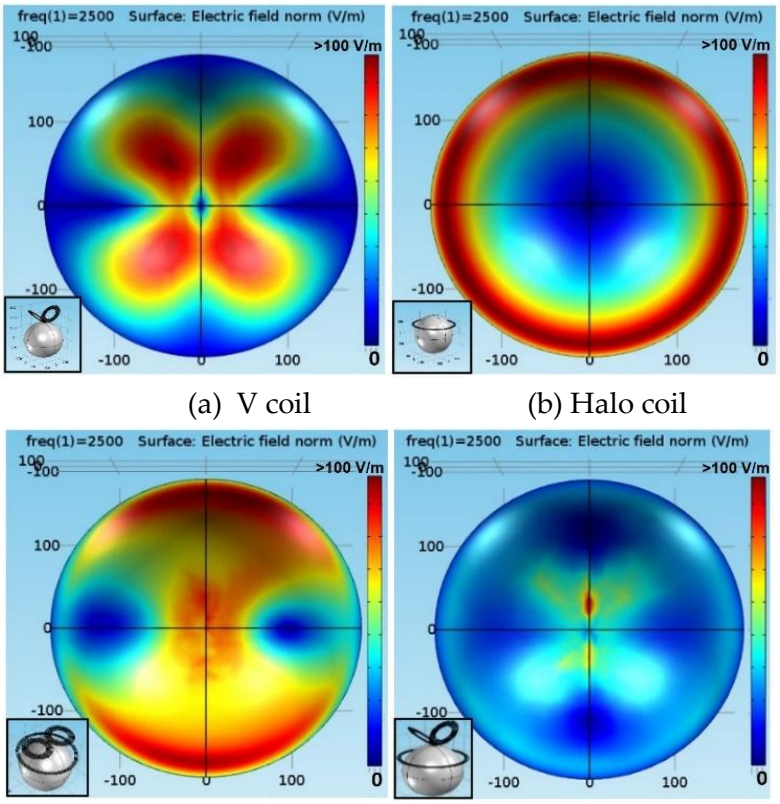

(a) V coil (b) Halo coil

(c) HFA coil (d) HVA coil

Fig. 3.7 Comparison of the surface electric field distribution of different coils.

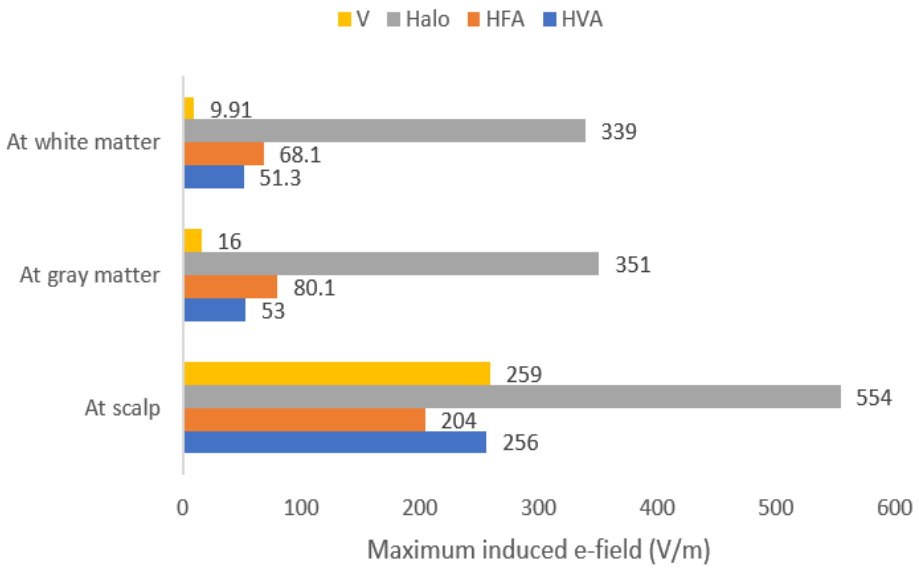

Fig. 3.8 Comparison of the maximum induced electric field on the scalp, gray matter, and white matter of head model for the V, Halo, HFA, and HVA coils.

Furthermore, the performance of the HVA coil in terms of focality is also evaluated to ensure the probability of stimulating the targeted neurons. The focality, $S_{1/2}$ calculation is performed by using the following equations [34]:

$$S_{1/2} = \frac{V_{1/2}}{D_{1/2}} \quad (5)$$

where $V_{1/2}$ (V-half) represents the volume within which the electric field is greater than half of E-Max, and $D_{1/2}$ is the distance from the mid-scalp to the white matter. For both single and assembly coils, the values of V-half and E-Max are presented as bar plot in Fig. 3.9. From the values of the V-half, it can be shown that the HVA coil has a lower volume of stimulation over three coils. Therefore, the reduced volume of stimulation reduces the value of $S_{1/2}$ which results in an increase focusing performance of the HVA coil.

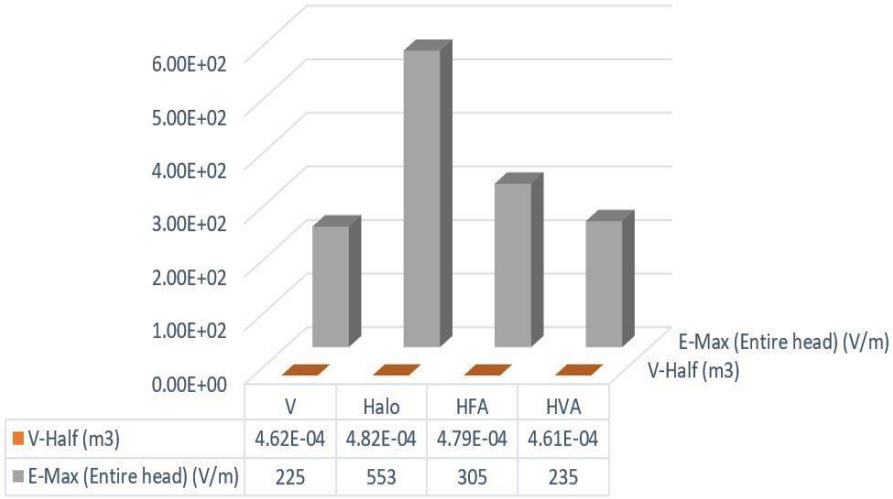

	V	Halo	HFA	HVA
V-Half (m3)	4.62E-04	4.82E-04	4.79E-04	4.61E-04
E-Max (Entire head) (V/m)	225	553	305	235

Fig. 3.9 Focality measurement of single and assembly coils in terms of V-Half and maximum electric field.

Chapter 4: DNN-BASED ELECTRIC FIELD PREDICTION MODEL

This chapter introduces the electric field prediction model approach with the aid of DNN. Moreover, the process of data generation, preprocessing followed by final electric field prediction from HVA TMS coil using DNN model is described comprehensively.

The system architecture of the proposed DNN based prediction model is shown in Fig. 4.1. The input and output of the proposed DNN model are the coil design parameters and the induced electric field respectively. The inner configuration of the DNN model with three non-linear hidden layers build a complex relationship between input parameters and output electric field. The details of the electric field prediction steps are described in the subsections below.

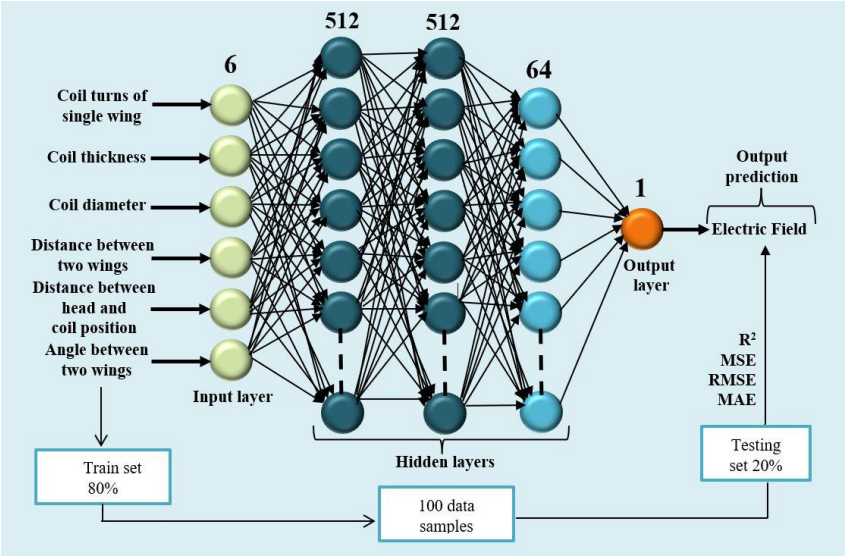

Fig. 4.1 System architecture of proposed DNN based model for electric field prediction.

4.1 DATASET CREATION

Fig. 4.2 illustrates the cross-section of the two-shell human head model with a halo-V assembly (HVA) coil configuration. The head model is comprised of two different anatomical layers including the skull and tissue fluid. Both layers are indicated in the inset of the three-dimensional head model in the Cartesian coordinates system. The outer and inner radius of the skull structure are 85 mm and 80 mm respectively, while the inner part of the skull i.e., the fluid tissue region is modeled with a radius of 80 mm. The HVA stimulation coil consists of two coils including halo coil and V coil. These two coils have a different number of turns such as: 9 for both wings of the V coil and 5 for the halo coil which makes a total of 23 turns. The V coil part of the HVA coil is placed at a distance of 5 mm from the vertex of the head model. Similarly, the halo coil part is placed at 90mm from the vertex of the head model. The design parameters of the HVA coil are summarized in Table 4.1. Each of the coils is modeled by considering the torus shape of copper material with an electrical conductivity of 5.8×10^7 S/m. The electromagnetic properties of materials implicated in this model are listed in Table 4.2 [35, 36]. For coil excitation, a current pulse with the high amplitude of 5000A and low-frequency of 2500 Hz are applied in the coil domain.

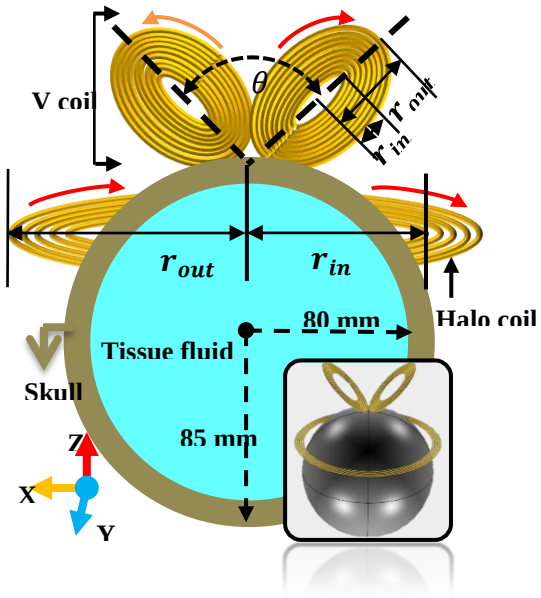

Fig. 4.2 Configuration of HVA coil. The red and green arrow lines indicate the clockwise and anti-clockwise current direction respectively.

Table 4.1 Geometrical parameters of the HVA coil.

Coil name		Inner radius r_{in} (mm)	Outer radius r_{out} (mm)	Total coil turns	Angle between two wings θ (degree)
HVA	V	27.5	47.5	18	45^0
	Halo	87.5	97.5	5	-

Table 4.2. Electromagnetic properties of coil material and anatomical layers at an operating frequency of 2500Hz.

Material	Conductivity [S/m]	Relative permittivity	Relative permeability
Skull	0.02	30380	1
Tissue fluid	4	80	0.99
Copper	5.8×10^7	1	0.99

Table 4.3 Interpretation of input and output features.

Inputs and outputs	Features to form model (unit)	Range
Input	Coil turns of single wing	1-15
	Coil thickness (mm)	0.1-0.9
	Coil diameter (mm)	60-110
	Distance between two wings (mm)	0.5-10
	Distance between head and coil position (mm)	1-15
	Angle between two wings (degree)	5-90
Output	Electric field (v/m)	130-300

For two shell head model (h), the electric fields, E_n are computed for six different parameters of HVA coil including coil turns of single wing (x_1), coil thickness (x_2), coil diameter (x_3), distance between two wings (x_4), distance between head and coil position (x_5), and angle between two wings (x_6). The variation of the values of each input parameter are summarized in Table 4.3. The dataset is obtained by setting D: = $\{h, [x_1; x_2; \ldots.; x_6]_n, E_n\}_{n=1}^N$ with a total of N=100 samples. Here, $\{E_n\}_{n=1}^N$ is found from $\{h, [x_1; x_2; \ldots.; x_6]_n\}_{n=1}^N$ under the

low frequency of 2500Hz and high amplitude of 5000A current pulse conditions. All the data samples are collected from COMSOL Multiphysics software in .csv format for the processing with the proposed DNN model.

4.2 DATA PRE-PROCESSING

Data preprocessing is an important part to increase the model prediction accuracy. This section gives a technical specification of the data preprocessing steps for our proposed prediction model. Moreover, the statistical analysis is conducted for a better understanding of the dataset, cleaning unwanted data, normalizing the features, and spliting the dataset. The histogram plots of features are shown in Fig. 4.3 to understand the distribution of each attribute independently. Among all input features, the coil thickness and coil diameter are negatively skewed and they have a great impact on the prediction model. The correlation between two quantitative attributes is visualized based on the correlation matrix heatmap as shown in Fig. 4.4. Analysis of correlation matrix provides six important unique input features such as coil turns of single wing, coil thickness, coil diameter, distance between two wings, distance between head and coil position, and angle between two wings of coil that are more correlated with the outputs feature of electric field. Fig. 4.5 indicates that the strong relationship between the attributes gives a high correlation value whereas hardly related attributes provide low correlation value. Moreover, the scatterplot matrix shown in Fig. 4.6 provides information about the structured relationship between the attributes. From the first row of the scatter plot matrix, it is obvious that the scatter plot of the output electric field is the function of all input features. Similarly, each input feature is the function of the output electric field as presented in other rows. The join distributions of three input features (i.e., coil turns of the single wing, coil thickness, coil diameter) and output feature (i.e., electric field) are shown diagonally in the scatterplot matrix. The statistical analyzes based on mean, standard deviation, minimum, and

maximum values are conducted to examine the feature-wise values that are summarized in Table 4. From this table, it is seen that the range of each feature is different from others. The minimum and maximum ranges of all features are set to a considerable value to remove bad working points. All the input and output features in the dataset are in numeric forms as continuous measurement data. Consequently, the normalization technique is applied for numeric features prior to training the proposed DNN model. The normalization technique coerces the values of all features into a distribution centered around 0 with a standard deviation of 1 by precomputing the mean and variance of the features as shown in Table 4.4. The numeric original feature and the corresponding normalized features are depicted in Fig. 4.7.

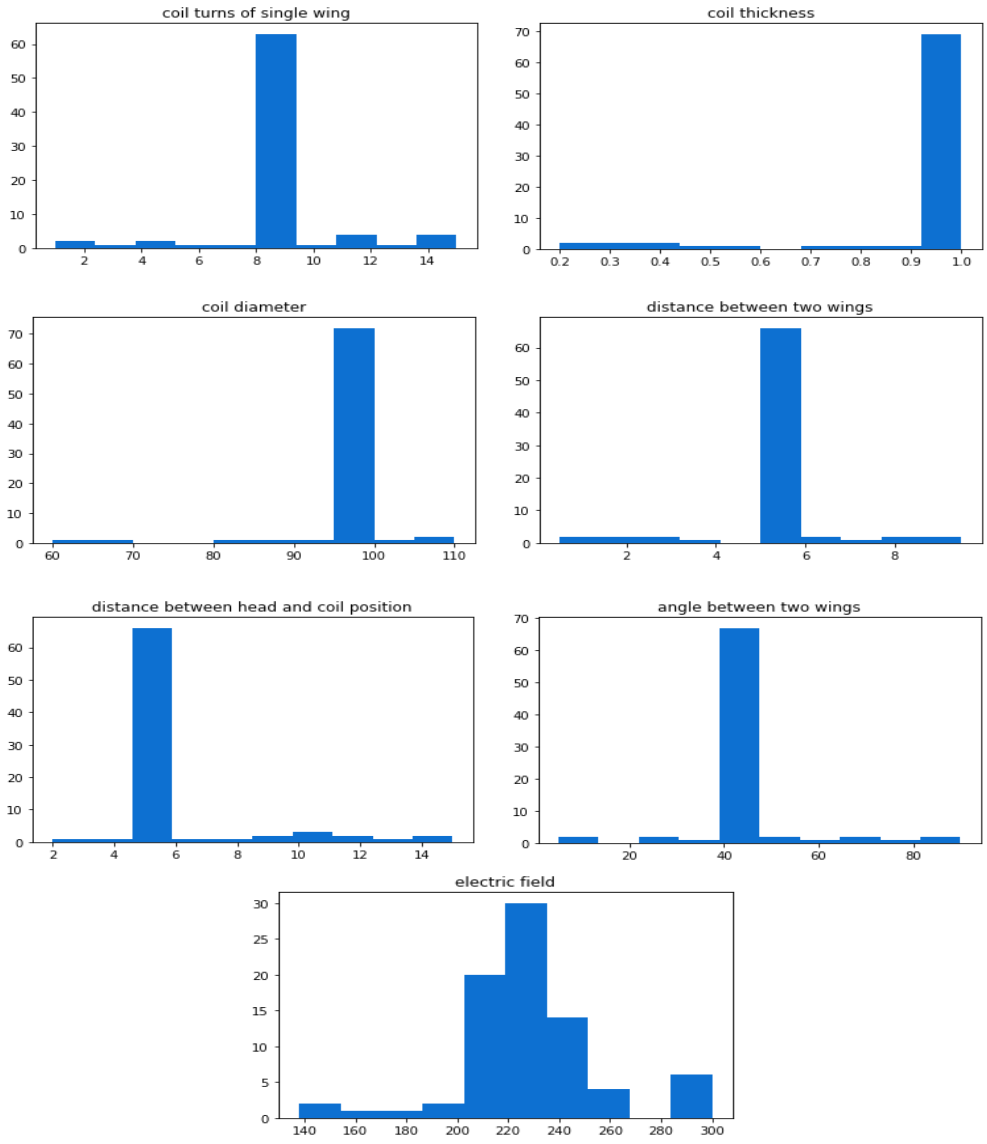

Fig. 4.3 Histogram for original feature visualization.

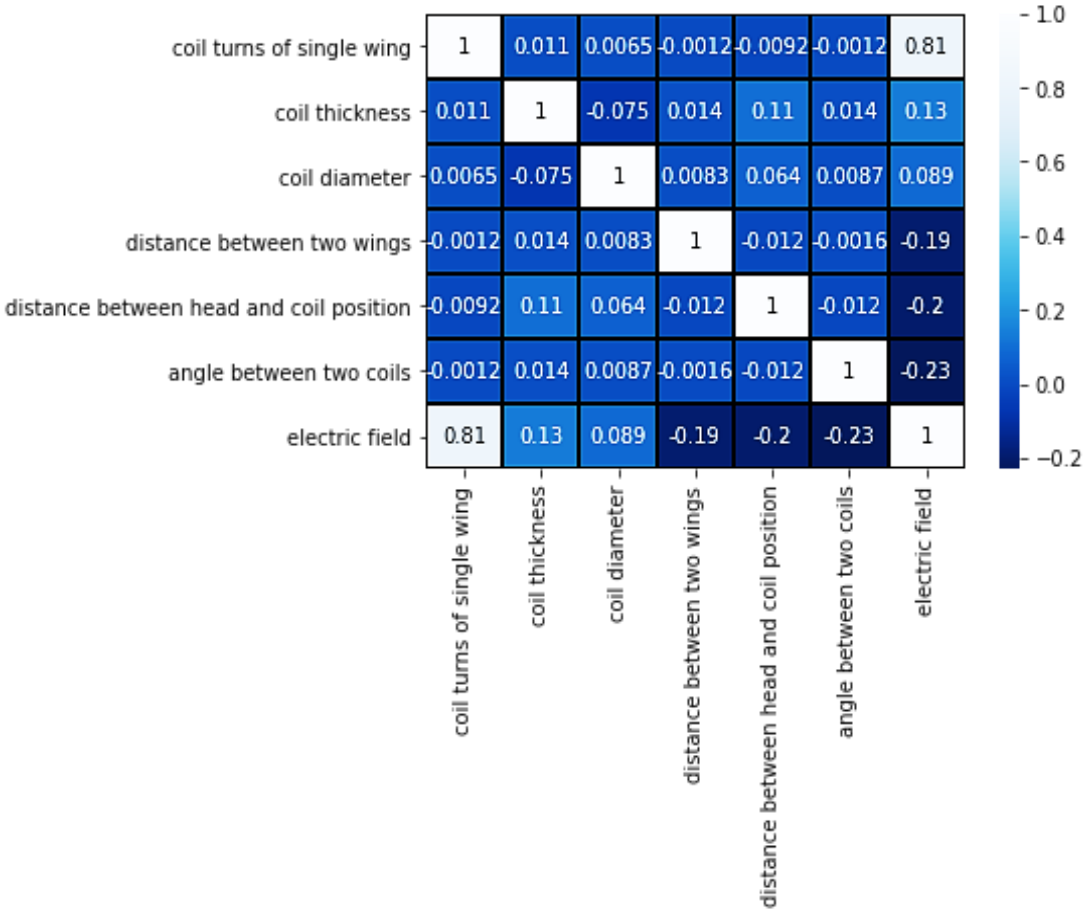

Fig. 4.4 Correlation matrix heatmap of attributes.

Table 4.4 statistical values of input and output features

Features	Mean	Standard Deviation	Min	Max
Coil turns of single wing	9.02	2.16	1.00	15.00
Coil thickness	0.93	0.19	0.20	1.00
Coil diameter	94.18	5.93	60.00	110.00
Distance between two wings	4.99	1.32	0.50	9.50
Distance between head and coil position	5.81	2.32	2.00	15.00
Angle between two wings	45.94	11.08	5.00	90.00
Electric field	229.87	31.26	138.00	329.00

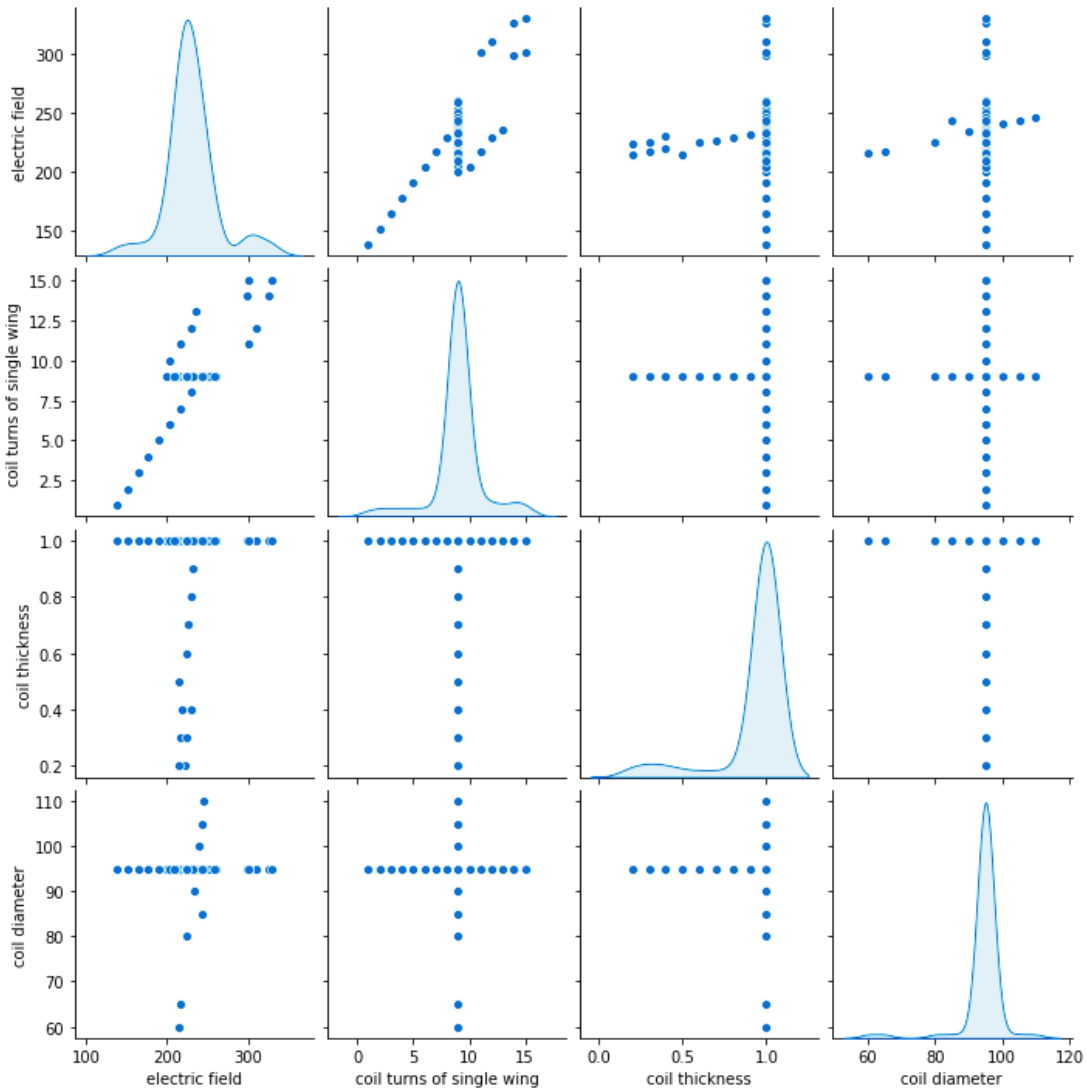

Fig. 4.5 Scatterplot matrix of features.

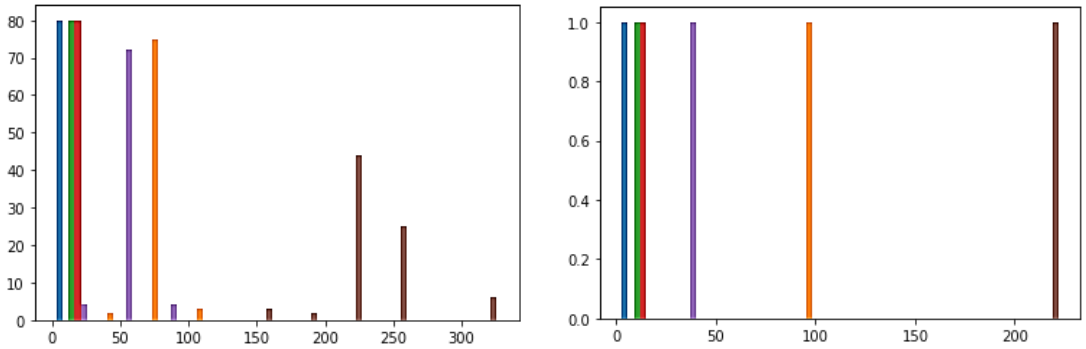

(a) Original input features with numeric value. (b) Input features after normalization.

Fig. 4.6 Numeric input feature and its normalization.

4.3 DNN PREDICTION MODEL

In a DNN model, the number of nodes in hidden input and output layers are identical to the numbers of input and output features [37]. However, the number of nodes and hidden layers can be varied depending on the complexity of the problem and the data set. The proposed DNN model architecture as shown in Fig. 4.8 comprises of an input layer with six nodes, three fully connected (dense) hidden layers with 512-512-64 nodes for the first, second, and third layers respectively, and an output dense layer with one node for the prediction of electric field, E_{pred}. The electric field value can be calculated by using equation (5) as:

$$E_{pred} = \text{Linear}\left[ReLU_{1,2,3 \in h}\left(\begin{bmatrix} x_1 \\ x_2 \\ \vdots \\ x_6 \end{bmatrix} \bullet W_{i,j}^{(k)} + b_i^{(k)} \right) \right] \quad (5)$$

where $W_{i,j}^{(k)}$ is the weight connecting to the *i*th unit in *k*th hidden layer and *j*th unit of previous layer, and $b_i^{(k)}$ is the bias connecting the *i*th unit in the *k*th hidden layer. A non-linear transfer function called rectified linear unit (ReLU) is selected for the hidden layers that provides a non-linearity to the DNN regression model. ReLU is defined as:

$$ReLU\,(P_h) = \max\,(0, P_h) \quad (6)$$

$$\textit{Where,} \qquad P_h = \begin{bmatrix} x_1 \\ x_2 \\ \vdots \\ x_6 \end{bmatrix} \bullet W_{i,j}^{(k)} + b_i^{(k)} \quad (7)$$

A linear transfer function is also assigned for the output layer to predict the single electric field value. The mean absolute error loss function is chosen for the model to determine the optimum values of trainable parameters such as weight, $W_{i,j}^{(k)}$ and bias, $b_i^{(k)}$. Then, the Adam optimizer is selected with a default learning rate of 0.001 to minimize the loss function [38]. The optimizer minimizes the loss function by updating the trainable parameters with its

gradients that are found by the backpropagation method. The entire dataset used for the model is divided into two sets with an amount of 80% for the training, and the residual 20% for testing.

4.4 RESULTS

In this work, the 6-512-512-64-1 DNN model with 299,150 trainable parameters achieve the best performance for the purpose of electric field prediction. Table 4.5 summarizes the results of four verification matrices such as coefficient of determination (R^2), mean squared error (MSE), mean absolute error (MAE), and root mean squared error (RMSE), which are commonly used to analyze the model prediction. Equations (8) to (12) are employed to define the four above-mentioned metrics. Here, y_{true} indicates the true output, y_{pred} indicates the predicted output, and the mean of the ground truth output is represented as y_{mean}. The total number of data is denoted as n.

$$y_{mean} = \frac{1}{n}\sum_{k=1}^{n} y_{true} \tag{8}$$

$$R^2 = 1 - \frac{\sum_{k=1}^{n}(y_{true}-y_{pred})^2}{\sum_{k=1}^{n}(y_{true}-y_{mean})^2} \in [0,1] \tag{9}$$

$$MSE = \frac{\sum_{k=1}^{n}(y_{true}-y_{pred})^2}{n} \tag{10}$$

$$MAE = \frac{\sum_{k=1}^{n}|y_{true}-y_{pred}|}{n} \in [0,+\infty] \tag{11}$$

$$RMSE = \sqrt{\frac{\sum_{k=1}^{n}(y_{true}-y_{pred})^2}{n}} \in [0,+\infty] \tag{12}$$

Layer (type)	Output Shape	Param #
normalization	(None, 6)	13
dense (Dense)	(None, 512)	3584
dense (Dense)	(None, 512)	262656
dense (Dense)	(None, 64)	32832
dense (Dense)	(None, 1)	65

Total params: 299,150

Fig. 4.8 Proposed DNN model architecture.

The R^2 metric represents the quality of the proposed DNN regression model. It determines how well the model predicts the electric field value. To perfectly fit the data of the regression prediction model, the value of R^2 is considered to be equal to 1. However, the regression loss function, MSE is calculated by summing the squared of distances between the true value and predicted value. The value of MSE=0 is preferable. Another loss function called MAE is measured by averaging all absolute errors. RMSE is also calculated by the square root of the sum of square deviation of true and predicted values over the total number of data n. For perfectly fitting the predicted values to the true values, the RMSE=0 is desirable.

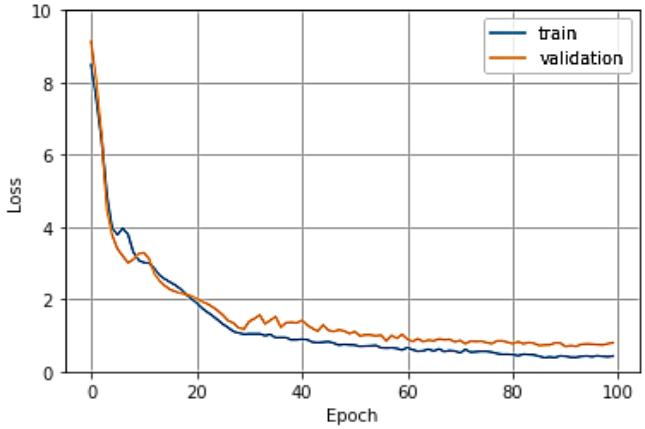

Fig. 4.9 Loss versus epoch plot for the DNN model.

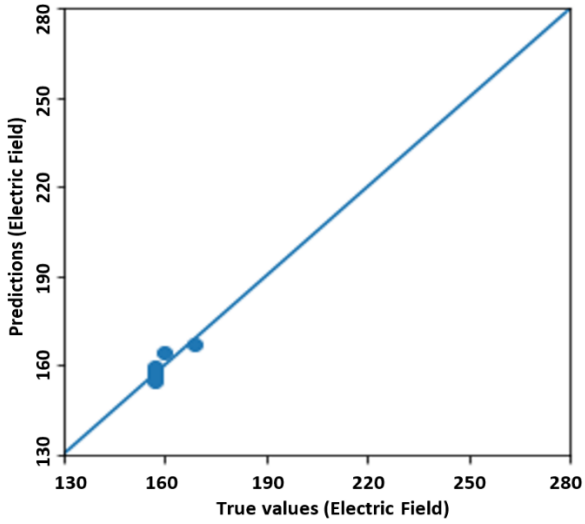

Fig. 4.10 The predicted electric field values versus simulated data on test set.

The training process of the proposed DNN model against 100 iterations (epochs) is shown in Fig. 4.9, in which the training and validation loss are found equal at 20 epochs. After 20 epochs, both errors are started to decrease at an optimum level and the finest result is achieved within the epochs of 90 to 100.

Table 4.5 Results of four verification matrices

R^2	MSE	MAE	RMSE
0.766	0.184	0.262	0.429

The predicted electric field values are plotted against true electric field values (simulated values) for the proposed model which is shown in Fig. 4.10. The graph indicates that the prediction accuracy of the proposed DNN model is good enough as the predicted electric field values are quite similar to the simulated electric field values. Therefore, the proposed model has the capability to predict the electric field values ranging from 130 V/m to 300 V/m in an accurate manner. Moreover, the prediction accuracy of the model as a function of single input feature (i.e., coil turns of single wing) is shown in Fig. 4.11. For a range of values of input feature, there is a considerable number of accurate predictions of the electric field values of the HVA TMS coil under high amplitude and low-frequency current conditions.

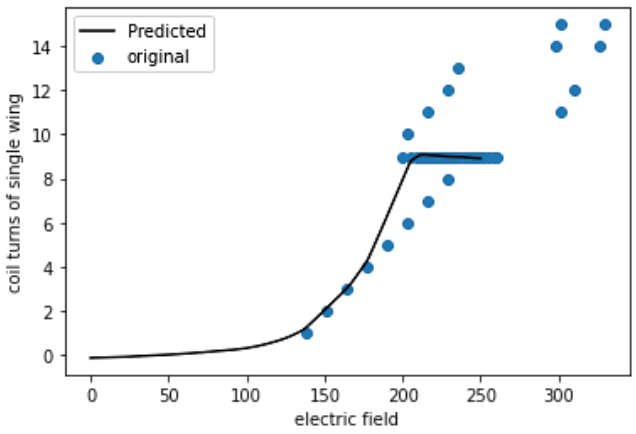

Fig. 4.11 The predicted electric field values as a function of the single input feature of coil turns of single wing.

4.5 DISCUSSION

The main advantage of the proposed DNN model is that it can estimate the induced electric field in a head model much faster way than the electric field determination process by an EM software. The electric field computational time for the proposed DNN model and simulation software are determined. Table 4.6 represents the computation time to estimate the induced electric field in a head model from a HVA TMS coil. The expected values of computation time using GPU and CPU for the proposed DNN model are found 0.04 s and 1.98 s respectively. On the other hand, the required computation time for COMSOL Multiphysics software is found 6 min 15 s even though this estimated time exclude the construction time of anatomical head and coil model. If the construction time of anatomical head and coil model is considered then it will be few hours.

Table 4.6 Computation time to estimate electric field for HVA TMS coil.

Model	Computation time
DNN (GPU)	0.04 s
DNN (CPU)	1.98 s
Simulation software (Excluding coil and anatomical head modeling)	6 min 15 s

Chapter 5: ATTENTION-ASSISTED IMPROVED ELECTRIC FIELD PREDICTION MODEL

This chapter describes an improved DNN approach to concern about improving electric field prediction accuracy. A comprehensive description of each individual network with a final attention component is presented. Moreover, the performance of the improved DNN model is compared with the existing prediction model for finding the model's effectiveness in HVA TMS coil-induced electric field prediction.

5.1 ATTENTION-ASSISTED DNN MODEL

The architecture of the proposed attention-based hybrid 1D CNN-BiLSTM for electric field prediction is shown in Fig. 5.1. The process of prediction is started by generating a dataset with the composition of input and target features. Where the input features are the composition of six coil design parameters of the HVA coil and the target feature is the induced electric field. After that, the raw dataset is fed into 1D CNN network for feature extraction by applying three consecutive 1D Conv layers with a kernel size of 2×1. Subsequently, a fully connected layer with 16 nodes is used for the vectorial representation of the features. Then, the sequential model called Bi-LSTM is utilized to learn the valid information from the feature maps by using forward and backward hidden states. Later on, an attention layer is performed that merged important features and chooses the critical features by redistributing the weights. Finally, a fully connected layer is used for electric field prediction.

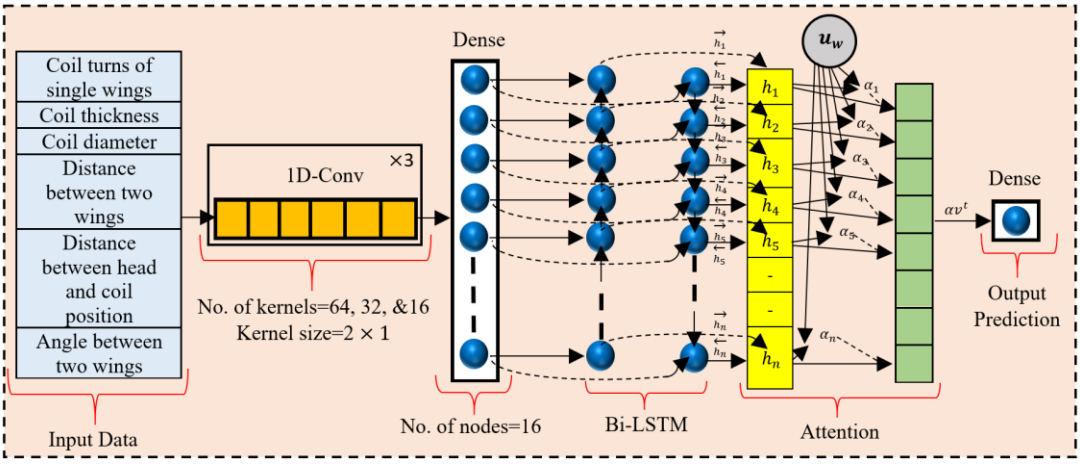

Fig. 5.1 Overview of the proposed electric field prediction network architecture comprising attention mechanism in the hybrid 1D CNN-BiLSTM model.

After creating the dataset, the preprocessing technique such as normalization is employed before feeding into the final prediction model. The normalization technique smooths the training time of the network by converting all the numerical values in the range of 0 and 1. Then, the normalized data are used for further processing through the proposed prediction model that follows the following sequential steps:

1. *1D CNN Model*

The utilization of 1D CNN model on the normalized continuous numerical data can extract a representative and effective feature by performing a one-dimensional convolution operation with multiple filters. To match the one-dimensional characteristics of the continuous numerical data, the 1D convolutional filters and feature maps are employed for the CNN model. By applying more than one number of convolutional layers, the 1D CNN model deepens the feature extraction process. Thus a higher level of features after performing more than one convolutional operation makes the prediction task more robust and discriminative. Initially, the preprocessed normalized data with a shape of (6 × 1) is used as the input of the 1D CNN model. Then, the input data is passed through three consecutive 1D convolutional (Conv) layers to extract

deep features, where each of the Conv layers contains 64, 32, and 16 1D kernels respectively with a size of (2 × 1). After performing the Convolution operation, a rectified linear unit (ReLU) activation function is utilized which introduces non-linearity in the model and reduces the overfitting problem as well. The operation of the 1D Conv layer followed by ReLU activation function is performed as follows:

$$y_j^{(k)} = ReLU_{1,2,3\in h}\left[\sum_{i=1}^{N_{(k-1)}} Conv1D\left(x_i^{(k-1)}, W_{i,j}^{(k)}\right) + b_j^{(k)}\right] \quad (5)$$

where, the i^{th} feature map in the $(k-1)^{th}$ layer is represented as $x_i^{(k-1)}$ and the j^{th} feature map in the k^{th} layer is represented by y_j^k. Moreover, the trainable convolutional kernel is denoted as $W_{i,j}^{(k)}$and $N_{(k-1)}$ denotes the total number of feature maps in the $(k-1)^{th}$ layer. The 1D convolution operation without zero-padding is performed on $x_i^{(k-1)}$ and $W_{i,j}^{(k)}$. Therefore, the dimension reduction of the feature maps is found at the $(k-1)^{th}$ layer than the k^{th} layer. In addition, the bias of the j^{th} feature map in the k^{th} layer is represented as $b_j^{(k)}$. The operation of ReLU activation function is performed as follows:

$$ReLU\,(P_h) = max\,(0, P_h) \quad (6)$$

where,

$$P_h = \sum_{i=1}^{N_{(k-1)}} Conv1D\left(x_i^{(k-1)}, W_{i,j}^{(k)}\right) + b_j^{(k)} \quad (7)$$

After passing through all the 1D convolutional layers, the obtained 16 feature maps with the size of (4 × 1) are fed into one dense layer with 16 nodes. Then, the output features are fed into the Bi-LSTM model for finding valid information from the feature maps.

2 . Bi-directional LSTM Model

As the dataset is composed of some sort of noisy numerical data, the prediction of the electric field from the noisy data is complex. For electric field estimating and eliminating the noise, the Bi-LSTM network is adopted to the 1D CNN model. The Bi-directional LSTM network is a two-way stacked LSTM network with forwarding and backward LSTM features. The previous values are learned

through the forward LSTM network in the forward direction, and similarly, the future values are learned in the reverse direction by applying a backward LSTM network. The utilization of hidden states in the latter layer help to learn both forward and backward information. The mathematical equation for performing this task through the Bi-LSTM unit is explained as follows:

$$\overrightarrow{h_n} = \sigma\left(W_1 x_t + W_2 \overrightarrow{h_{n-1}}\right) \times tanh(C_t) \quad (8)$$

$$\overleftarrow{h_n} = \sigma\left(W_3 x_t + W_4 \overleftarrow{h_{n-1}}\right) \times \tanh(C_t') \quad (9)$$

$$h_n^{[p]} = W_5 \overrightarrow{h_n} + W_6 \overleftarrow{h_n} \quad (10)$$

where, x_t is the input at time t. W's are the weights of gates of LSTM cells. $\overrightarrow{h_n}$ and $\overleftarrow{h_n}$are the forward and backward outputs, respectively. The generated Bi-LSTM features from the i^{th} features in the p^{th} layer is denoted as $h_n^{[p]}$ that keeps information in Bi-directional steps. In this paper, the generated feature vector of 1D CNN and dense are fed to the Bi-LSTM model. An activation function of $'tanh'$ is adopted to finish normalization and help to reduce the overfitting problem.

3 . Attention Mechanism

Generally, all the parameters in the input data do not contribute equally to deciding whether the parameter belongs to a particular prediction. Therefore, the utilization of the attention mechanism is performed to emphasize the most important parameters during prediction. In the attention mechanism, the weight, α_n for each individual Bi-LSTM feature, $h_n^{[p]}$ is assigned with a focus on output labels. Mathematically, the followings are computed for the attention function:

$$\mu_i = tanh(W_d \times flatten\left(h_n^{[p]}\right) + b) \quad (11)$$

$$\alpha_n = \frac{exp(\mu_i\, u_w)}{\sum_n exp(\mu_i\, u_w)} \quad (12)$$

$$\alpha v^t = \sum_n \alpha_n\ h_n^{[p]} \quad (13)$$

Here, $h_n^{[p]}$ is the feature vector obtained in the BiLSTM layer, which is passed to a one-layer neural network (p=1) to get the μ_i as a hidden representation of $h_n^{[p]}$.

The W_d and b are weight matrix and bias vector respectively that are initialized during the neural network training. The influence of the important parameters can be measured by calculating the similarity between μ_i and u_w. Where, u_w is randomly initialized feature vector. Afterward, a normalized weight, α_n is obtained by using the softmax function for each input feature. The attention weights, $\sum_n \alpha_n$ should be equal to 1. The larger the weight of α_n the more significant the feature for prediction. Finally, the attentive feature αv^t is fed to a dense layer consisting of one neuron. The predicted output, E_{Pred} can be represented as:

$$E_{Pred} = Linear\ (\sum_j W_{kj} \times\ \alpha v_j^t +\ b_k) \tag{14}$$

where, W_{kj} and b_k are represented as the weight matrix, and bias vector respectively. The activation function '*linear*' is added to the proposed model for final electric field prediction. The entire network architecture's properties with their specification and the number of required parameters are demonstrated in Table 5.1 In this work, the attention-based model with 6,641 trainable parameters acquires the best performance for the prediction of the induced electric field.

4. Model validation

To validate the proposed attention-based hybrid 1D CNN-BiLSTM model, the ten-fold cross-validation method is utilized that randomly divides the overall data into ten approximately equal sections. Then, each time one portion from the splitted sections is selected as the test set, and the rest of the portions are considered as the training set. At every iteration, the model is trained using data shuffling. Finally, the estimation of the model evaluation matrices is performed by taking an average of ten predicted results. The summary of the ten-fold cross-validation methods is depicted as follows:

- Partitioning the raw dataset into ten parts containing an equal number of numerical values in each part.
- One part is selected as the test set for each iteration, and the remaining

dataset is utilized as a training set to train the model.

- After training, the results of ten iterations are averaged to obtain the final test results.

Table 5.1. Layer properties of proposed attention-based hybrid 1D CNN-BiLSTM model.

Layer No.	Layer Name	Feature size	Specification	Parameter
1	Input	6 × 1	-	0
2	1D Convolutional	6 × 64	Filter size: 2×1 Filter number: 64	192
3	1D Convolutional	5 × 32	Filter size: 2×1 Filter number: 32	4128
4	1D Convolutional	4 × 16	Filter size: 2×1 Filter number: 16	1040
5	Dense	4 × 16	-	272
6	Bi-LSTM	4 × 8	Hidden units: 4	672
7	Attention	16	Units: 16	320
8	Dense	1	-	17
				Total=6,641

Table 5.2. Hyper-parameters setting of the proposed model.

Hyper-parameter	Value
Loss function	Mean absolute error
Initial learning rate	0.01
Epochs	100
Optimizer	Adam

The selection of optimum hyperparameter values is important to train the proposed prediction model for superior results. Table 5.2 represents the optimal values of the hyperparameters of the proposed attention-assisted hybrid 1D CNN-BiLSTM model. The model is compiled using an Adam optimizer with an initial learning rate of 0.01. Moreover, the model training is performed for 100 epochs per fold. The mean absolute error is chosen as a loss function to compute model loss. For conducting training and testing of the proposed

model, the Google Colab platform is used with Python version 3.7.13. The Model is implemented using Keras = 2.8.0 and TensorFlow = 2.8.2 framework. The Pandas= 1.3.5 and Sklearn =1.0.2 packages have been used for data preparation and evaluation respectively. During the training, the model occupied 1.43 GB of RAM and 38.58 GB of disk space in the Colab environment.

5.2 RESULTS AND PERFORMANCE EVALUATION

All the values of the performance evaluation matrices are summarized in Table 5.3. It is clear from Table 5.3 that the values are almost equal to their preferable values. According to the preferable values of all the performance matrices, it can be said that the proposed attention-assisted 1D CNN-Bi-LSTM model shows superior induced electric field prediction with a minor number of errors in the testing data. Moreover, Fig. 5.2 plots the proposed model training process in terms of MAE, MSE, and RMSE against 100 iterations (epochs), in which the finest result is achieved after 80 epochs for regression performance evaluation.

Table 5.3. Performance evaluation matrices for electric field prediction task.

R^2	MSE	MAE	RMSE
0.9992	0.0005	0.0188	0.0228

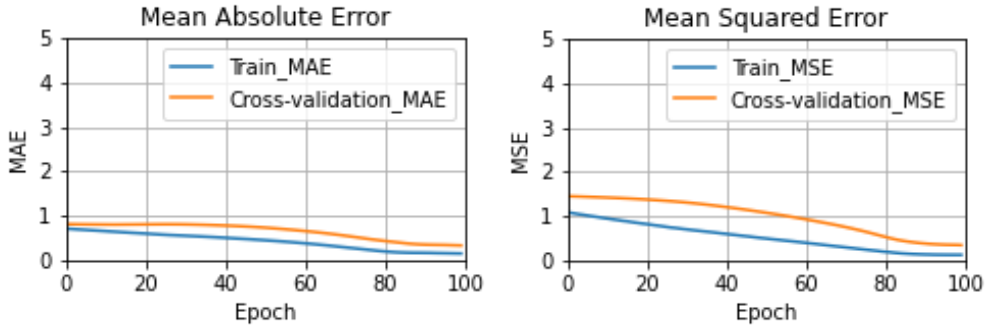

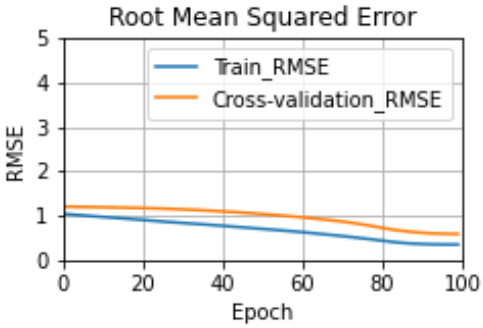

Fig. 5.2 Performance evaluation on attention-assisted 1D CNN-BiLSTM model: MAE, MSE, and RMSE.

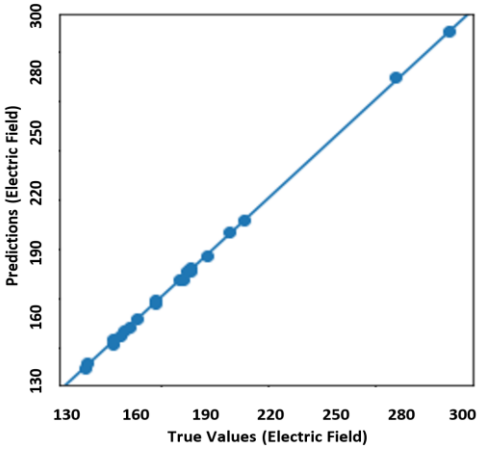

Fig. 5.3 Scatter plot of predicted electric field values versus actual data on the test set.

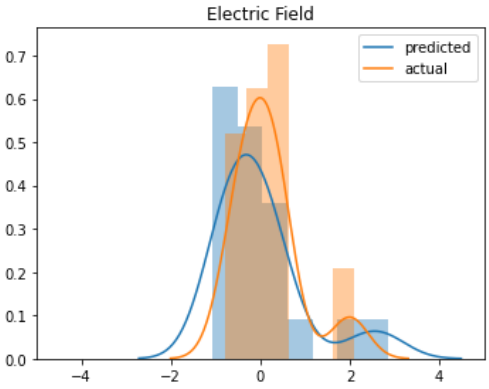

Fig. 6. KDE probability density curve of eletric field: actual vs. predicted.

Fig. 5.3 represents the scatter plot of predicted electric field values against simulated (ground truth) electric field values for the proposed attention-based model. From this graph, it can be seen that all the predicted electric field values are almost similar to the simulated electric field values that ensure good accuracy between attention-based model prediction and simulated data

prediction. For this reason, the proposed model is capable of enumerating induced electric field values in a correct manner ranging from 130 V/m to 300 V/m. Moreover, the Kernel Density Estimation (KDE) is illustrated in Fig. 5.4 to estimate and compare the predicted electric field values with the actual electric field values on the test set in a probability density distribution manner. According to the performance of the prediction model, the KDE probability density curve of predicted electric field values agrees well with the actual electric field values. It is recognized that the proposed prediction model attains a superior performance on the test set.

5.3 DISCUSSION

The prediction accuracy, R^2 of different possible regression models such as 1D CNN, BiLSTM, 1D CNN-BiLSTM, 1D CNN with Attention, and BiLSTM with Attention on validation dataset is illustrated in Fig. 5.5. Among these DL models, the proposed model provides the highest electric field prediction accuracy of approximately 99.92%. In addition, the model performance is evaluated by comparing the proposed attention-based hybrid model with the state-of-the-art models as presented in Table 5.4. The works reported in [11, 12] used a single TMS coil type with a single coil parameter of coil position to enumerate the electric field. The main drawback of using a single TMS coil is a lack of tradeoff between focality and depth of stimulation [10]. For ensuring an efficient clinical treatment with minimum side effects, the presence of a tradeoff between focality and depth is needed. Therefore, in this study, the DNN based prediction of electric field from an assembly coil with different coil parameters is presented that meets the simulation tradeoff between depth and focality. However, the prediction model used in the work provides lower prediction accuracy in terms of R^2 value which is approximately 0.766. Moreover, other evaluation matrices such as MSE, RMSE, and MAE that represent losses of the prediction model are quite larger. For this reason, the improved DNN model

such as attention-based hybrid deep CNN-BiLSTM model ensures optimum prediction accuracy of 0.9992 in terms of R^2 value with the lowest computation time of 0.11 s. Thus, it can ensure optimum therapeutic efficacy such as effective and safe stimulation during treatment pertaining to several neurological disorders with optimum electric field prediction.

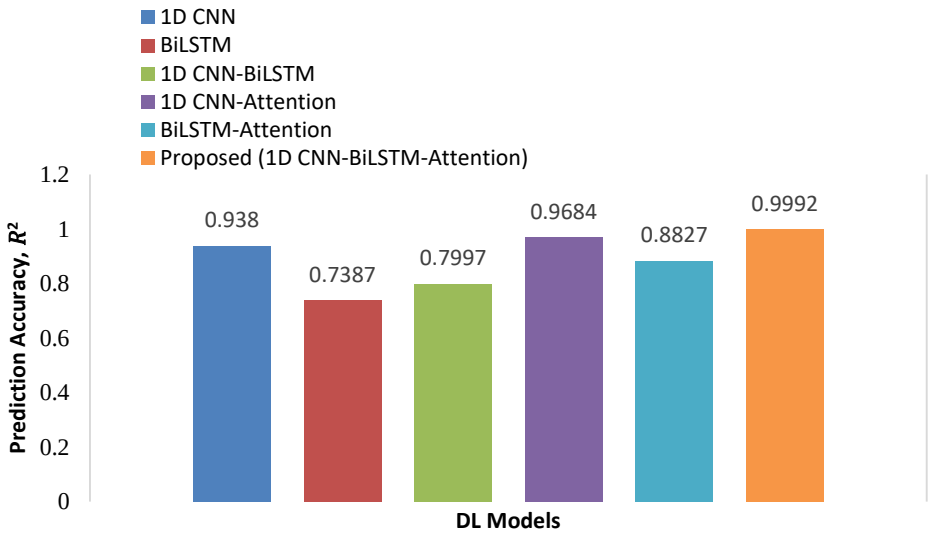

Fig. 5.5 The prediction accuracy of different models on the validation dataset.

Table 5.4. Comparison table of the proposed model with the existing related works.

Reference	[11]	[12]	This work	
Prediction model	U-Net	CNN	DNN	1D CNN-BiLSTM with Attention Mechanism
Data type	Unstructured: Image	Unstructured: Image	Structured: Numerical value	Structured: Numerical value
Number of datasets	261,072	800	100	100
Coil type	Single	Single	Assembly	Assembly
Coil parameter	coil position	-	coil position coil turns coil thickness coil diameter coil angle coil wings distance	coil position coil turns coil thickness coil diameter coil angle coil wings distance

Prediction task	Segmentation	Regression	Regression	Regression
Computational time	0.541 s	-	0.04 s	0.11 s
Performance evaluation matrix	CC=0.93 PSNR=29dB MAE=6 RMAD=6%	R^2 = 0.92 MAPE = 6.2%	R^2 = 0.766 MSE = 0.184 MAE = 0.262 RMSE = 0.429	R^2 = 0.9992 MSE = 0.0005 MAE = 0.0188 RMSE = 0.0228

Chapter 6: CONCLUSION AND FUTURE WORK

This chapter summarizes the contents discussed in the introduction, methodology, results, and discussion section without repetition. It contains general, key findings, conclusions, limitations, implication issues and future recommendations.

This work presents a regression model based on an 1D DNN model for predicting electric fields induced by HVA TMS coil. Without compromising the computational cost of electric field enumeration, the model improves the prediction accuracy by employing attention layer in the DNN model. The attention mechanism helps the model to predict electric field values from 130 to 300 V/m by impacting the most relevant parameters of the HVA coil. By feeding a lower-sized database of 100 samples, the model obtained reasonable prediction accuracy of $R^2 = 0.9992$ that ensures the capability of the model to enumerate electric field from HVA coil with varied coil designing parameters. Without requiring any three-dimensional mathematical model of human head phantom and TMS coil, the proposed method efficiently estimated electric field from a new unknown dataset in a very short time of 0.11 s. Therefore, to meet the requirement of the neurological disorder patients, the proposed attention-based model can aid the TMS manufacturer to design an optimum coil based on the predicted electric fields. In the future, a database with larger samples can be developed by considering several new assembly coils rather than single assembly coils to improve model generalization capability. Moreover, database can be developed based on the numeric data from the realistic anatomical head model to increase the practical feasibility of the work.

Bibliography

[1] F. Spagnolo *et al.*, "Bilateral Repetitive Transcranial Magnetic Stimulation With the H-Coil in Parkinson's Disease: A Randomized, Sham-Controlled Study," *Frontiers in neurology,* vol. 11, p. 584713, 2021.

[2] G. Schiena, E. Maggioni, S. Pozzoli, and P. Brambilla, "Transcranial magnetic stimulation in major depressive disorder: Response modulation and state dependency," *Journal of affective disorders,* vol. 266, pp. 793-801, 2020.

[3] S. L. Kletzel *et al.*, "Safety considerations for the use of transcranial magnetic stimulation as treatment for coma recovery in people with severe traumatic brain injury," *The Journal of head trauma rehabilitation,* vol. 35, no. 6, p. 430, 2020.

[4] M. Isserles *et al.*, "Deep Transcranial Magnetic Stimulation Combined with Brief Exposure for Post-Traumatic Stress Disorder–A Prospective Multisite Randomized Trial," *Biological Psychiatry,* 2021.

[5] O. Afuwape, P. Rastogi, and D. Jiles, "Comparison of the Effect of Coil Configuration and the Variability of Anatomical Structure on Transcranial Magnetic Stimulation," *IEEE Transactions on Magnetics*, 2020.

[6] M. Lu and S. Ueno, "Comparison of the induced fields using different coil configurations during deep transcranial magnetic stimulation," *PloS one,* vol. 12, no. 6, p. e0178422, 2017.

[7] T. Pashut *et al.*, "Mechanisms of magnetic stimulation of central nervous system neurons," *PLoS Comput Biol,* vol. 7, no. 3, p. e1002022, 2011.

[8] J. C. Lin, "Transcranial Magnetic Stimulation Therapy for Depression and Psychiatric Disorders [Health Matters]," *IEEE Microwave Magazine,* vol. 17, no. 8, pp. 23-93, 2016.

[9] S. Rossi, M. Hallett, P. M. Rossini, A. Pascual-Leone, and S. o. T. C. Group, "Safety, ethical considerations, and application guidelines for the use of transcranial magnetic stimulation in clinical practice and research," *Clinical neurophysiology,* vol. 120, no. 12, pp. 2008-2039, 2009.

[10] L. I. N. de Lara *et al.*, "A 3-axis coil design for multichannel TMS arrays," *NeuroImage,* vol. 224, p. 117355, 2021.

[11] T. Yokota *et al.*, "Real-time estimation of electric fields induced by transcranial magnetic stimulation with deep neural networks," *Brain stimulation,* vol. 12, no. 6, pp. 1500-1507, 2019.

[12] O. F. Afuwape, O. O. Olafasakin, and D. C. Jiles, "Neural Network Model for Estimation of the Induced Electric Field during Transcranial Magnetic Stimulation," *IEEE Transactions on Magnetics,* 2021.

[13] A. Kybartaite, "Computational representation of a realistic head and brain volume conductor model: electroencephalography simulation and visualization study," *International journal for numerical methods in biomedical engineering,* vol. 28, no. 11, pp. 1144-1155, 2012.

[14] M. Fuchs, M. Wagner, and J. Kastner, "Development of volume conductor and source models to localize epileptic foci," *Journal of Clinical Neurophysiology,* vol. 24, no. 2, pp. 101-119, 2007.

[15] E. A. Rashed, J. Gomez-Tames, and A. Hirata, "Deep learning-based development of personalized human head model with non-uniform conductivity for brain stimulation," *IEEE transactions on medical imaging,* vol. 39, no. 7, pp. 2351-2362, 2020.

[16] E. Dandıl, M. Çakiroğlu, Z. Ekşi, M. Özkan, Ö. K. Kurt, and A. Canan, "Artificial neural network-based classification system for lung nodules on computed tomography scans," in *2014 6th International conference of soft computing and pattern recognition (SoCPaR)*, 2014, pp. 382-386: Ieee.

[17] F. Shaukat, G. Raja, R. Ashraf, S. Khalid, M. Ahmad, and A. Ali, "Artificial neural network based classification of lung nodules in CT images using intensity, shape and texture features," *Journal of Ambient Intelligence and Humanized Computing,* vol. 10, pp. 4135-4149, 2019.

[18] V. A. Maksimenko *et al.*, "Artificial neural network classification of motor-related eeg: An increase in classification accuracy by reducing signal complexity," *Complexity,* vol. 2018, 2018.

[19] Z. Cömert and A. KOCAMAZ, "A study of artificial neural network training algorithms for classification of cardiotocography signals," *Bitlis Eren University journal of science and technology,* vol. 7, no. 2, pp. 93-103, 2017.

[20] M. Bataineh and T. Marler, "Neural network for regression problems with reduced training sets," *Neural networks,* vol. 95, pp. 1-9, 2017.

[21] I. I. Argatov and Y. S. Chai, "An artificial neural network supported regression model for wear rate," *Tribology International,* vol. 138, pp. 211-214, 2019.

[22] D. F. Specht, "A general regression neural network," *IEEE transactions on neural networks,* vol. 2, no. 6, pp. 568-576, 1991.

[23] Y. Raptodimos and I. Lazakis, "Using artificial neural network-self-organising map for data clustering of marine engine condition monitoring applications," *Ships and Offshore Structures,* vol. 13, no. 6, pp. 649-656, 2018.

[24] E. Sharghi, V. Nourania, A. AliAshrafia, and H. Gökçekuşb, "Monitoring effluent quality of wastewater treatment plant by clustering based artificial neural network method," *Desalination and Water Treatment,* vol. 164, pp. 86-97, 2019.

[25] M. Matos, S. Pinho, and V. Tagarielli, "Predictions of the electrical conductivity of composites of polymers and carbon nanotubes by an artificial neural network," *Scripta Materialia,* vol. 166, pp. 117-121, 2019.

[26] Y. L. Zhukovskiy, N. Korolev, I. Babanova, and A. Boikov, "The prediction of the residual life of electromechanical equipment based on the artificial neural network," in *IOP Conference Series: Earth and Environmental Science*, 2017, vol. 87, no. 3, p. 032056: IOP Publishing.

[27] F. Mohamadian, L. Eftekhar, and Y. Haghighi Bardineh, "Applying GMDH artificial neural network to predict dynamic viscosity of an antimicrobial nanofluid," *Nanomedicine Journal,* vol. 5, no. 4, pp. 217-221, 2018.

[28] Z. An, S. Li, J. Wang, Y. Xin, and K. Xu, "Generalization of deep neural network for bearing fault diagnosis under different working conditions using multiple kernel method," *Neurocomputing,* vol. 352, pp. 42-53, 2019.

[29] S. Zibman, G. S. Pell, N. Barnea-Ygael, Y. Roth, and A. Zangen, "Application of transcranial magnetic stimulation for major depression: coil design and neuroanatomical variability considerations," *European Neuropsychopharmacology*, 2019.

[30] C. F. Sabottke and B. M. Spieler, "The effect of image resolution on deep learning in radiography," *Radiology. Artificial intelligence*, vol. 2, no. 1, 2020.

[31] A. M. Jafari and A. Abdolali, "Adopting reciprocity theorem in deep transcranial magnetic stimulation problem to design an efficient single source coil array based on nerve cell direction," *Medical & biological engineering & computing*, vol. 56, no. 1, pp. 13-23, 2018.

[32] O. F. Afuwape, J. Boldrey, P. Rastogi, S. A. Bentil, and D. C. Jiles, "Influence of brain–scalp distance on focality of the quadruple butterfly coil for transcranial magnetic stimulation," *IEEE Transactions on Magnetics*, vol. 57, no. 2, pp. 1-4, 2020.

[33] A. L. Benabid, S. Chabardes, J. Mitrofanis, and P. Pollak, "Deep brain stimulation of the subthalamic nucleus for the treatment of Parkinson's disease," *The Lancet Neurology*, vol. 8, no. 1, pp. 67-81, 2009.

[34] C. Liu, H. Ding, X. Fang, and Z. Wang, "Optimal design of transcranial magnetic stimulation thin core coil with trade-off between stimulation effect and heat energy," *IEEE Transactions on Applied Superconductivity*, vol. 30, no. 4, pp. 1-6, 2020.

[35] H. Hallez *et al.*, "Dipole localization errors due to not incorporating compartments with anisotropic conductivities: Simulation study in a spherical head model," *International Journal of Bioelectromagnetism*, vol. 7, no. 1, pp. 134-137, 2005.

[36] C. Gabriel, *Complication of the dielectric properties of body tissues atRF and microwave frequencies*. Dept. Phys., King's College London, London, U.K., Brooks Air Force Tech. Rep. AL/OE-TR-1996-0004, 1996.

[37] W. Liu, Z. Wang, X. Liu, N. Zeng, Y. Liu, and F. E. Alsaadi, "A survey of deep neural network architectures and their applications," *Neurocomputing*, vol. 234, pp. 11-26, 2017.

[38] D. P. Kingma and J. Ba, "Adam: A method for stochastic optimization," *arXiv preprint arXiv:1412.6980*, 2014.